Progress in Natural Science: Materials International 30 (2020) 545–551

HOSTED BY

Contents lists available at ScienceDirect

Progress in Natural Science: Materials International

journal homepage: www.elsevier.com/locate/pnsmi

Compositional complexity dependence of dislocation density and mechanical properties in high entropy alloy systems

P. Thirathipviwat[a,b], G. Song[c], J. Bednarcik[d,e], U. Kühn[a], T. Gemming[a], K. Nielsch[a,f,g], J. Han[a,h,*]

[a] Leibniz Institute of Solid State and Materials Research (IFW Dresden), Helmholtzstr. 20, 01069, Dresden, Germany
[b] Frontier Research Center for Applied Atomic Sciences, Ibaraki University, Tokai, Japan
[c] Division of Advanced Materials Engineering and Institute for rare metals, Kongju National University, Cheonan, Chungnam 330-717, Republic of Korea
[d] Institute of Physic, Pavol Jozef Safarik University in Košice, 041 54, Košice, Slovakia
[e] Deutsches Elektronen-Synchrotron (DESY), Notkestraße 8, D-22607, Hamburg, Germany
[f] Institute of Materials Science, Technische Universität Dresden, TU Dresden, 01062, Dresden, Germany
[g] Institute of Applied Physics, Technische Universität Dresden, TU Dresden, 01062, Dresden, Germany
[h] Korea Institute for Rare Metals, Korea Institute of Industrial Technology (KITECH), Incheon, 21999, Republic of Korea

ARTICLE INFO

Keywords:
High entropy alloys
Dislocation density
Synchrotron XRD
Mechanical properties

ABSTRACT

This study focuses on a quantitative analysis of dislocation accumulation after cold plastic deformation and mechanical properties of FeNiCoCrMn and TiNbHfTaZr high entropy alloys (HEAs) which are single phase *fcc* and *bcc* solid solutions, respectively. In order to study the role of compositional complexity from unary to quinary compositions on dislocation accumulation and mechanical properties after plastic deformation, the single solid solution phase forming sub-alloys of the two HEAs were investigated. All studied samples revealed a large plastic deformability under cold-rotary swaging process by 85–90% area reduction without intermediate annealing. The dislocation density of all studied samples, determined by Williamson-Hall method on synchrotron X-ray diffraction patterns, were between 10^{14} - 10^{15} m^{-2} dependent on the alloy composition. The level of dislocation density after plastic deformation is not only affected by the number of constituent element but the lattice distortion and intrinsic properties in terms of stacking fault energy, modulus misfit, and melting point also impact the dislocation storage. The level of dislocation density determines the level of mechanical properties because of a resistance to dislocation motions. The hardness and yield compressive strength of the studied samples are proportional to the level of dislocation density.

1. Introduction

Nowadays “High entropy alloys (HEAs)” are becoming a common term in the metallurgy world because their microstructure and unique properties have attracted a lot of attention in the scientific research and industrial application [1,2]. HEAs, firstly proposed by two independent research works in 2004 [3,4], are generally known to form a single solid solution phase with relatively simple crystal structure, such as face-centered cubic (*fcc*) structure, body-centered cubic (*bcc*) structure as well as hexagonal close-packed (*hcp*) structure in which different atom species are randomly placed. Alloying strategy for HEAs is based on entropic stabilization associated with multiple major constituent elements in near- or equi-atomic ratio. This strategy is different from conventional alloys that generally consist of one major element with or without minor alloying elements. Early publications of HEAs suggested that high configuration entropy leads to a microstructure stabilization [1]. In fact, it has been recently reported that many HEAs consist a meta-stable phase and the solid solution phase is not stable at all temperature [2]. However, a solid solution phase plays a main role in their unique properties, especially mechanical properties such as high strength and excellent fracture toughness due to a mutual interaction between multiple major elements of HEAs [5,6].

The mixing of different atom species in the solid solution causes special features, such as lattice distortion and sluggish diffusion. It is often suggested that the high strength of HEAs is mainly a result of solid solution hardening associated with compositional heterogeneity [7,8]. Due to the absence of intermetallic compound, HEAs demonstrate outstanding ductility, and high malleability [9]. This allows significant improvement of strength for the HEA by cold work hardening. For example, yield strength of *fcc*-structured FeNiCoCrMn HEA increases from 200 MPa to 1000 MPa by 50% cold working [10]. It is a result of an assumption that a high degree of compositional heterogeneity has a

* Corresponding author.
E-mail addresses: jhan@kitech.re.kr, jhhan0523@gmail.com (J. Han).

https://doi.org/10.1016/j.pnsc.2020.07.002
Received 16 January 2020; Received in revised form 26 June 2020; Accepted 27 July 2020
Available online 30 August 2020

great important role in impeding dislocation motions during plastic deformation [7]. The deformation mechanism of HEAs is expected to be different from conventional concentrated solid solution alloys. Many studies in literatures demonstrated that the plastic deformation of HEAs is facilitated by conventional deformation mechanism e.g. dislocation gliding and/or twinning [11,12]. For instance, in *fcc* FeNiCoCrMn HEA, the planar glide of $a/2 < 110 >$ dislocations on {111} planes dominate the early stage deformation at a broad range of temperature (77–873K) [13]. However, the quantitative analysis on dislocation accumulation in HEAs are limited in literatures. In order to understand the deformation behavior and mechanical properties of HEAs, the level of dislocation density is needed to be correlated with the role of compositional complexity.

Due to high malleability, good microstructure and thermal stability [7], many series of HEAs are produced by conventional solid-state synthetic methods and fabrication routes [14]. This advantage lead to wide-ranging studies on an interplay between microstructure and properties of HEAs [1]. The rotary swaging is a conventional plastic deformation process and widely used for practical applications, such as drive shafts of automobile components [15]. The rotary swaging gives many advantages, e.g. near-net-shape profiling, good surface finish and high-throughput mass production, which lead to cost-effective production. During the swaging process, the oscillating movement of the dies with a high frequency facilitates high plastic strain in a single processing step. This prevents brittle failure at early stage deformation and enables higher accumulation of plastic strain [14]; therefore, the rotary swaging is a good option to be used for a study in a work hardening of HEAs.

In this work, the dislocation density after plastic deformation was evaluated for *fcc*-structured FeNiCoCrMn and *bcc*-structured TiNbHfTaZr HEAs in a relation to their mechanical properties. In order to study the compositional complexity dependence of dislocation formation and accumulation during the cold working process, the single solid solution phase samples composed of different number constituent element(s); unary, binary, ternary, quaternary and quinary compositions were also investigated.

2. Experimental procedure

2.1. Sample preparation

The ingots of *fcc*-structured Fe-Ni-Co-Cr-Mn family alloys (equiatomic FeNiCoCrMn, FeNiCoCr, FeNiCo, FeNi alloys and pure Ni) and *bcc*-structured Ti-Nb-Hf-Ta-Zr family alloys (equiatomic TiNbHfTaZr, TiNbHfTa, TiNbHf, TiNb alloys) were fabricated by arc-melting the mixture of pure elements (purity higher than 99.9 wt%) and re-melted at least 3 times to ensure chemical homogeneity under a Ti-gettered high-purity argon atmosphere. As-received 2 mm diameter niobium rod was investigated for a comparison with the *bcc*-structured samples. These master ingots were subsequently transferred to an in-house built cold crucible levitation melting device for drop-casting into water-cooled copper mold of 6 mm diameter cylinder form. The cast rods were encapsulated in an evacuated and Ar backfilled quartz ampoules before homogenization (*fcc* samples: 1273 K for 12 h and *bcc* samples: 1373 K for 40 h) followed by water quenching. The homogenized rods were then subjected to rotary swaging process (HMP Heinrich Müller Maschinenfabrik GmbH.) at room temperature. The rods were cold-swaged by about 19% reduction of cross-sectional area per step until approximately 85% reduction of cross-sectional area for the *fcc* alloys and approximately 90% reduction for *bcc* alloys.

2.2. Evaluation of dislocation density

The dislocation density after cold swaging was examined by Williamson-Hall [16,17] and Williamson-Smallman methods [18] on the synchrotron X-ray diffraction patterns. The high energy synchrotron X-ray generates can penetrate deeper through the as-swaged 2 mm rods in order to yield a high statistic with the large number of data set and the short wavelength permits the study on a local structure [19]. High energy synchrotron X-ray diffraction patterns was captured in transmission geometry with $E = 60$ keV ($\lambda = 0.2067150$ Å) and $Q_{max} = 12$ Å^{-1} ($Q = 4\pi\sin\theta/\lambda$)at High Resolution Powder Diffraction Beamline P02.1 of the DESY in Hamburg, Germany. The crystallite size (D_v) and lattice strain (ε_{str}), which are two main sources contributing to peak broadening, can be calculated by Williamson and Hall equation as defined by the following equation:

$$\Delta\beta = \beta_D - \beta_{inst} = \beta_{size} + \beta_{strain} \quad (1)$$

$$\Delta\beta cos\theta = \lambda/D_v + 4\varepsilon_{str}(\sin\theta) \quad (2)$$

where β_D is an integral breadth of Bragg peak, and β_{inst}, β_{size} and β_{strain} are the integral breadths dependent on instrumental, crystallite size and strain effects, respectively. The instrumental broadening (β_{inst}) was measured using LaB6. From equation (2), the Williamson-Hall plot can be plotted between $(\beta_D - \beta_{inst})\cos\theta$ and $4\sin\theta$. The lattice strain (ε_{str}) and grain (crystallite) size (D_v) were derived from the slope and the y-intercept of the linear fit, respectively. The value of the lattice strain was used to evaluate the dislocation density (ρ) using the following equation of Williamson and Smallman [18];

$$\rho = k\frac{\varepsilon^2}{b^2} \quad (3)$$

where b is the magnitude of the Burgers vector and k is a constant value. The plastic deformation in the *fcc*-structured FeNiCoCrMn HEA is observed to occur by planar dislocation glide on the normal *fcc* slip system, $\{111\} < 110 >$ [11].It leads to an assumption that slip in all studied *fcc*-structured samples takes place in {111} octahedral planes and $< 110 >$ directions. For the studied *fcc*-structured samples, $k = 16.1$ is used for the calculation. In the *bcc*-structured TiNbHfTaZr HEA, it seems clear that plastic deformation mechanism at room temperature is similar to that of the conventional *bcc* metals where the motion of screw dislocation with $b = a/2 < 111 >$ Burgers vector is dominant [12]. The k value for the calculation in all studied *bcc*-structured samples is 14.4.

2.3. Mechanical properties

The mechanical properties were determined by micro Vickers hardness (Shimadzu HVM-2000) and compression test (Instron 5869). The microhardness was examined with applied test load of 200 g for 10 s. The value of hardness for each sample was averaged from at least 15 indents. For the compression test, the test specimen in a form of cylindrical rod with height to diameter ratio of 2:1 was compressed at a strain rate of 5×10^{-4} s^{-1}. The strain was measured by a laser extensometer (Fiedler Optoelektronik).

3. Results and discussion

3.1. Dislocation density after cold working

3.1.1. fcc phase Fe-Ni-Co-Cr-Mn family alloys

Fig. 1(a) presents the high energy synchrotron X-ray diffraction patterns of *fcc* Fe-Ni-Co-Cr-Mn family alloys after 85% area reduction. The XRD patterns of all as-swaged *fcc* samples demonstrate a single *fcc* structure phase. The XRD peak positions are shifted to low angle of 2θ with alloying from unary to quinary compositions, indicating an expansion of the lattice parameter. The lattice parameters of the Ni, FeNi, FeNiCo, FeNiCoCr and FeNiCoCrMn were determined as 3.5210, 3.5834, 3.5695, 3.5709 and 3.5931 Å, respectively. Williamson-Hall plot calculated by integral breadths and 2θ positions of the reflection planes (111), (002), (022), (113), (222), (004), (133), (024), (224), (115) and (004) is presented in Fig. 1(b). The crystallite (grain) size and

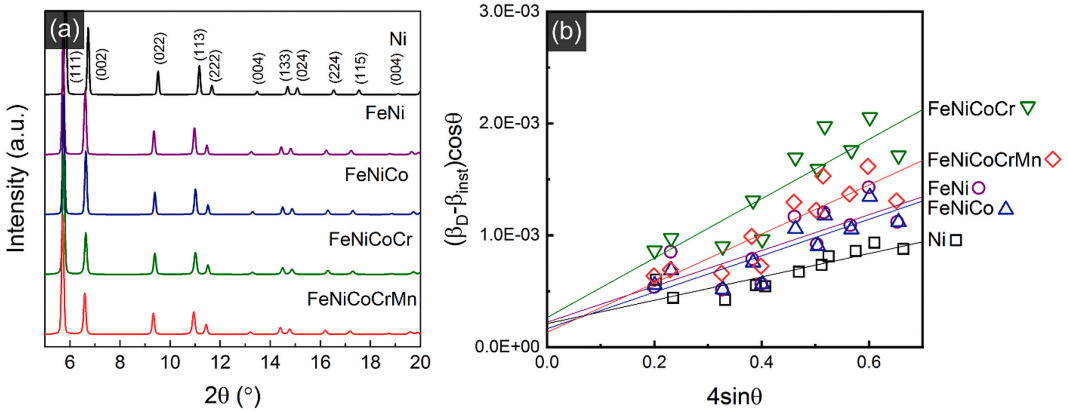

Fig. 1. (a) High energy synchrotron X-ray diffraction patterns and (b) Williamson-Hall plots of the as-swaged *fcc* Fe-Ni-Co-Cr-Mn family samples.

Table 1
Lattice parameters (a), crystallite size (D_v), lattice strain (ε), dislocation density (ρ), shear modulus (G), melting point and homologous temperature (T/T_m; T = 298K) of the as-swaged *fcc* Fe-Ni-Co-Cr-Mn family samples and the as-swaged *bcc* Ti-Nb-Hf-Ta-Zr family samples.

Alloys	a (Å)	D_v (nm)	ε (%)	ρx 10^{15} (m^{-2})	G** (GPa)	T_m (K)	T/Tm
Ni	3.521	98	0.104	0.28	76	1728 [6]	0.173
FeNi	3.583	93	0.160	0.64	78	1703 [6]	0.175
FeNiCo	3.570	125	0.163	0.67	77	1713 [6]	0.174
FeNiCoCr	3.571	78	0.266	1.78	87	1693 [6]	0.176
FeNiCoCrMn	3.593	156	0.220	1.20	84	1562 [6]	0.191
Nb*	3.298	116	0.170	0.510	38	2750 [20]	0.108
TiNb	3.281	137	0.211	0.794	41	2346**	0.127
TiNbHf	3.370	185	0.358	2.167	37	2399**	0.124
TiNbHfTa	3.355	152	0.350	2.089	45	2622**	0.114
TiNbHfTaZr	3.398	120	0.412	2.823	43	2524 [6]	0.118

*As-received rod, **Calculated by the rule of mixture and melting temperature of each constituents obtained from reference [20].

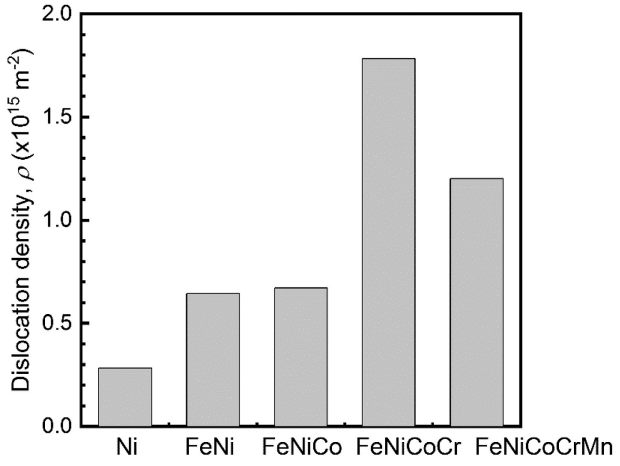

Fig. 2. Dislocation density accumulation in the as-swaged *fcc* Fe-Ni-Co-Cr-Mn family samples.

lattice strain were extracted from the plot and summarized in Table 1. The grain size for the deformed *fcc*-structured samples were very fine between 78 and 156 nm due to a large degree of cold deformation. The magnitudes of the lattice strain (ε_{str}) were 0.104, 0.160, 0.163, 0.266 and 0.220% for Ni, FeNi, FeNiCo, FeNiCoCr and FeNiCoCrMn specimens, respectively.

According to equation (3), the dislocation density after cold-swaging is calculated by the values of the lattice strain. The dislocation densities of the samples after 85% area reduction were summarized in Table 1 and Fig. 2. The dislocation densities of the Ni, FeNi, FeNiCo, FeNiCoCr and FeNiCoCrMn samples were 0.28 × 10^{15}, 0.64 × 10^{15}, 0.67 × 10^{15}, 1.78 × 10^{15} and 1.20 × 10^{15} m^{-2}, respectively. This calculation for dislocation density of the FeNiCoCrMn HEA and its sub-alloys in this study seems reliable because these magnitudes of dislocation density are within the range of the reported values between 10^{15} - 10^{16} m^{-2} for pure metals and conventional alloys after plastic deformation [18].

Our previous study demonstrated that the dislocation accumulation during plastic deformation is related to the compositional complexity and stacking fault energy of alloys [21]. It can be seen from Fig. 2 that the increase in compositional complexity increased the level of dislocation density. An increase in compositional complexity enhances point defects and the atomic-level heterogeneity. These obstacles impede dislocation movement and thus facilitate dislocation accumulation. Besides the compositional heterogeneous, the lattice distortion is often considered in an issue of the interaction between defects and dislocation. However, a recent report presented that the lattice of the FeNiCoCrMn HEA is not severely distorted and similar to Ni metal in the level of distortion [22,23]. In order to anticipate the level of lattice distortion, the atomic size misfit can be determined the lattice distortion [23]. The atomic size misfits of the studied *fcc* alloys are small in the range of 0.6–1.2% because of similar atomic sizes of their constituent elements. As the result, the role of lattice distortion has a minimal impact on the dislocation accumulation for the *fcc*-structured samples. Moreover, the alloying decreases in stacking fault energy (SFE) that determines the level of dislocation storage [24]. The low stacking fault energies leads to a large degree of dislocation dissociation and a difficulty of cross-slip and climb of dislocation [24]. The values of stacking fault energy for the studied *fcc*-structured samples are collected from previous experimental and computational studies [23]; 120 - 130 mJ/m^2 of pure Ni, 79 mJ/m^2 of FeNi, 31 mJ/m^2 of FeNiCo, 25 mJ/m^2 of FeNiCoCr and 18 - 27 mJ/m^2 of the FeNiCoCrMn HEA. The quaternary FeNiCoCr and quinary FeNiCoCrMn alloys can accumulate larger dislocation density during the plastic deformation because of their relatively lower SFE values.

As shown in Fig. 2, a significant change in the dislocation density between the ternary FeNiCo alloy and the quaternary FeNiCoCr alloy was observed. This is due to the addition of Cr which shows relatively higher elastic modulus among the constituent elements. The values of the shear modulus (G) for the FeNiCoCr (87 GPa) and FeNiCoCrMn (84 GPa) are relatively higher than the other samples (76-78 GPa), as presented in Table 1. One point can be mentioned that the dislocation density in the FeNiCoCrMn HEA is smaller than in the quaternary FeNiCoCr alloy; it is against the expectation because of higher compositional complexity and lower value of SFE in the FeNiCoCrMn HEA. After Mn addition to the FeNiCoCr alloy, the melting point of

FeNiCoCrMn is dropped to 1562 K from 1693 K of FeNiCoCr alloy. The significant decrease in melting point of FeNiCoCrMn HEA leads to a large difference in homologeous temperatures between the FeNiCoCr and FeNiCoCrMn alloys. The homologous temperature relates to a level of thermal energy available during the deformation. All samples were deformed at room temperature (T = 298 K), but at different homologous temperatures (T/T_m) due to their different melting temperature (T_m). Ni, FeNi, FeNiCo and FeNiCoCr have similar melting temperature ranging between 1693 and 1728 K, while that of the FeNiCoCrMn HEA is 1562 K, as listed in Table 1. The higher homologeous temperature allows larger level of thermal energy available in the FeNiCoCrMn HEA during the deformation. During cold plastic deformation of the FeNiCoCrMn HEA, larger level of thermal energy available in the sample promotes a more chance for dislocations motions to overcome the lattice resistance and move easily. The ease of dislocation motions in the FeNiCoCrMn HEA results in lower level of dislocation storage than the FeNiCoCr alloy. The other parameters (compositional complexity, atomic size misfit, SFE and shear modulus) involved in a determination of dislocation accumulation are not significantly different and can be considered to give a minimal effect on a decrease in dislocation density of the FeNiCoCrMn HEA.

3.1.2. *bcc* phase Ti-Nb-Hf-Ta-Zr family alloys

The synchrotron XRD patterns of the as-swaged *bcc* Ti-Nb-Hf-Ta-Zr family samples in Fig. 3(a) show the formation of a single body-centered cubic (*bcc*) structure phase for all studied samples. The lattice parameters were calculated as 3.298, 3.281, 3.370, 3.355 and 3.398 Å for Nb, TiNb, TiNbHf, TiNbHfTaZr, respectively. Fig. 3(b) shows the Williamson-Hall plot using integral breadths and 2θ positions of reflection planes (011), (002), (112), (022), (013), (222), (123), (033), (114), (024), (223) and (224). The lattice strain and grain size, which were interpreted from the Williamson-Hall plot, are listed in Table 1. All *bcc*-structured samples exhibited very fine grain sizes ranging between 116 and 185 nm due to the heavy deformation. The values of the lattice strain were determined as 0.170, 0.211, 0.358, 0.350 and 0.412% for Nb, TiNb, TiNbHf, TiNbHfTa and TiNbHfTaZr alloys, respectively. The lattice strain increases as the chemical complexity increases.

Fig. 4 shows the dislocation densities of the as-swaged *bcc* Ti-Nb-Hf-Ta-Zr family samples; 0.510×10^{15}, 0.794×10^{15}, 2.167×10^{15}, 2.089×10^{15} and 2.823×10^{15} m^{-2} for the Nb, TiNb, TiNbHf, TiNbHfTa and TiNbHfTaZr alloys. These magnitudes correspond to the values of plastically deformed alloys reported in literatures [18] as mentioned in the previous section of *fcc* phase Fe-Ni-Co-Cr-Mn family alloys. The dislocation density is a function of lattice strain as shown in equation (3). The lattice distortion is evident in TiNbHfTaZr HEA simulated by a supercell model based on density functional theory (DFT) [25]. The lattice distortion was reported to relate to the magnitude of

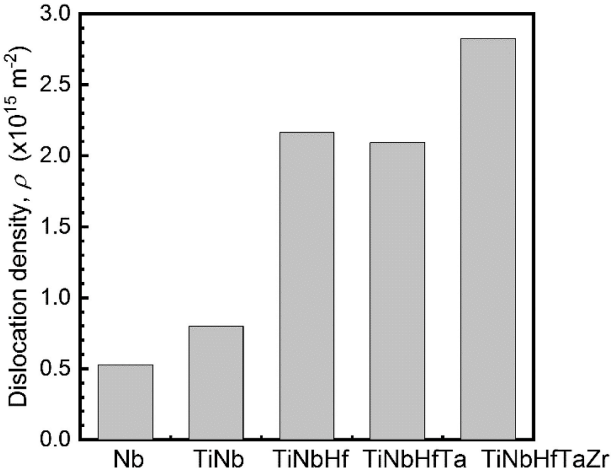

Fig. 4. Dislocation density accumulation in the as-swaged *bcc* Ti-Nb-Hf-Ta-Zr family samples.

atomic size misfit [23,24]. Among the constituent elements of the Ti-Nb-Hf-Ta-Zr family alloys, the atomic sizes of Hf (158 p.m.) and Zr (160 p.m.) are larger than those of Ti, Nb and Ta ranging 143 -146 p.m. The relatively larger atomic size differences in TiNbHf, TiNbHfTa and TiNbHfTaZr alloys eventually lead to higher dislocation density in TiNbHf, TiNbHfTa and TiNbHfTaZr compared to those of TiNb and Nb. The atomic size misfits of TiNb, TiNbHf, TiNbHfTa and TiNbHfTaZr samples are 1.12, 4.28, 4.13 and 4.98%, respectively, which are larger than the magnitudes of atomic size misfit of the *fcc* alloys in this study. The large atomic size misfit induces strong stress fields that impede dislocation motion. The large atomic size misfit as well as concentrated heterogeneous matrix cause a large dislocation accumulation. The discrepancy of dislocation density between the TiNbHf and TiNbHfTa alloys is caused by similar levels of atomic size misfit. Although the chemical composition of TiNbHf alloy is less complex, the atomic size misfit is slightly larger than TiNbHfTa alloy. The larger atomic size misfit of the TiNbHf alloy leads to a slightly larger level of dislocation accumulation than the TiNbHfTa alloy. As demonstrated in Fig. 4, the TiNbHfTaZr HEA accumulated the largest dislocation density due to the largest atomic size misfit and the highest degree of compositional heterogeneity.

As discussed above, stacking fault energy (SFE) and homologous temperature were considered to play an important role in dislocation accumulation during cold deformation for *fcc*-structured specimens in this study. However, it seems that the role of SFE and homologous temperature are insignificant in dislocation accumulation for the *bcc*-structured Ti-Nb-Hf-Ta-Zr system due to their relatively higher SFE and homologous temperature. The SFE values of the constituents in the *bcc*

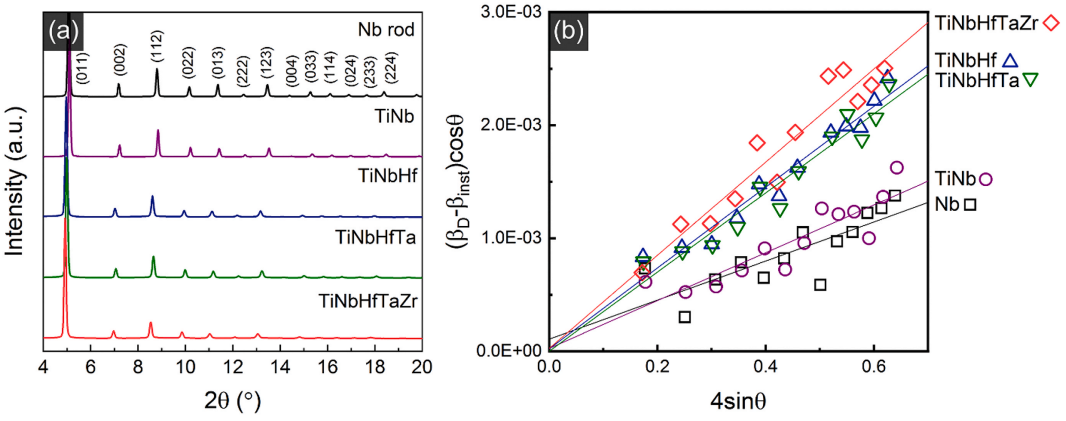

Fig. 3. (a) High energy synchrotron X-ray diffraction patterns and (b) Williamson-Hall plots the as-swaged *bcc* Ti-Nb-Hf-Ta-Zr family samples.

Ti-Nb-Hf-Ta-Zr system [24] are 200, 320, 390, 480 and 240 mJ/m^2 for Nb, Ti, Hf, Ta and Zr, respectively. In general, cross slip are favorable to accommodate deformation in high SFE materials [26]. Furthermore, less deformation twin is observed in *bcc* materials [6] and leads to a difficulty in plastic deformation and higher dislocation accumulation. The studied *bcc*-structured samples were cold-swaged at very low homologous temperatures (0.10–0.13) due to their high melting points between 2346 and 2750 K. As a result, the thermal energies available during the deformation could be less and similar for all *bcc* samples. Thus, all the *bcc* samples studied in the present research can be assumed to be similar in the thermal energies available during the deformation at room temperature. Hence, SFE and homologous temperature for the studied *bcc* samples lead to a slight effect on dislocation density.

3.2. Correlation between dislocation density and mechanical properties

In order to analyze the behavior of plastic deformation, Taylor proposed a model to predict the stress–strain response [27]. Many studies discuss that Taylor's model considers a plastic deformation of polycrystalline materials as agglomerates of single crystals and also ignores intergranular interactions between the grains. In case of large degree of plastic deformation, the plasticity behavior is successfully predicted by Taylor's model [28]. Taylor also describes the work hardening behavior by the relationship between flow stress and the total dislocation density. The strength of polycrystalline materials is controlled by dislocation density and interactions of dislocation movements. The work hardening is usually expressed by Taylor relationship [29]:

$$\sigma = \sigma_0 + M\alpha Gb\sqrt{\rho} \quad (4)$$

where σ is the true flow stress, σ_0 is the friction stress, G is the shear modulus, b is the magnitude of Burgers vector, α is a hardening parameter describing the average interactions between dislocations dependent on the alloy and M denotes Taylor factor. The magnitude of Taylor factor (M) is different dependent on material in terms of crystallographic active slip system and orientation texture [29]. Based on literatures, the FeNiCoCrMn HEA is deformed with the < 110 > slip direction; hence, the Taylor factor (M) is assumed to be 3.06 similar to typical *fcc*-structured polycrystalline materials [30]. In *bcc* metals, the numerous experiments demonstrate that slip occurs in the closet packed < 111 > direction. The Taylor factor (M), 2.754, is used in this calculation of the *bcc* samples for mixed slip modes in a < 111 > direction [31].

From equation (4), the mechanical properties of the studied alloys after deformation vary dependent on the level of dislocation density, shear modulus and Burgers vector. For each structure type of the samples, the magnitudes of shear modulus and Burgers vector are slightly different; therefore, the mechanical properties can be assumed to significantly depend on the level of dislocation density. Fig. 5 (a) and (b) present the correlation between mechanical properties (compressive yield strength and hardness) and dislocation density for the as-swaged *fcc* and *bcc* samples, respectively. The changes in compressive yield strength and hardness after the cold deformation are similar as a function of constituent elements number in both *fcc* and *bcc* alloy families. The levels of the compressive yield strength and hardness are proportional to the level of dislocation accumulations during the cold working rather than the number of constituent elements. Fig. 5 (a) demonstrates the mechanical properties of the *fcc* Fe-Ni-Co-Cr-Mn family alloys after 85% cross-sectional area reduction. Due to the highest degree of compositional heterogeneity, the FeNiCoCrMn HEA is expected to demonstrate the highest values of yield strength and hardness; however, the quaternary FeNiCoCr alloy shows the higher values. It indicates that the level of dislocation density determines the yield strength and hardness rather than the effect of element number. The more the dislocations are dense, the more the dislocation motions are impeded.

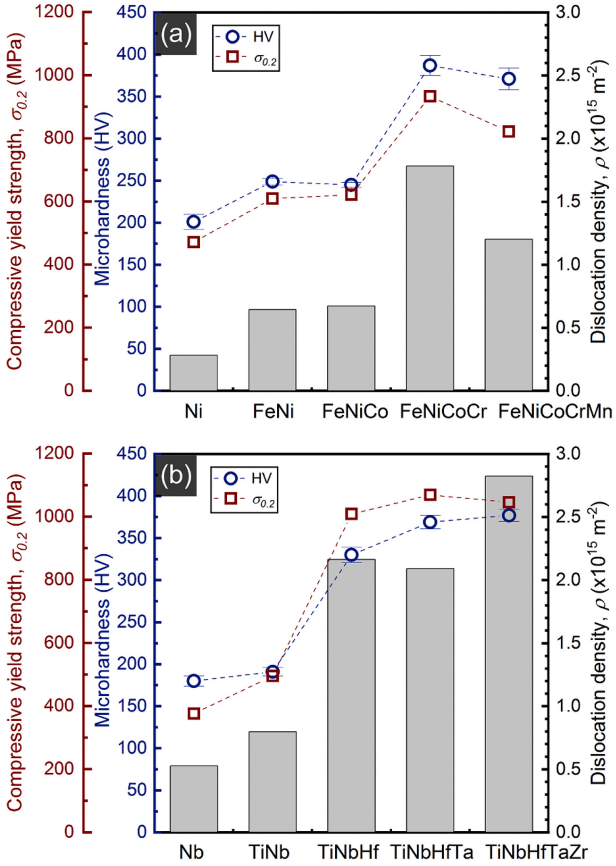

Fig. 5. Correlation between mechanical properties (compressive yield strength and hardness) and dislocation density for (a) the as-swaged *fcc* Fe-Ni-Co-Cr-Mn family samples and (b) the as-swaged *bcc* Ti-Nb-Hf-Ta-Zr family samples.

Table 2
Compressive yield strength ($\sigma_{0.2}$) and hardness of the as-swaged and as-annealed samples and calculation of hardness using rule of mixtures (ROM).

Alloys	As-swaged		As-annealed		Calculated by ROM
	$\sigma_{0.2}$ (MPa)	Hardness (HV)	$\sigma_{0.2}$ (MPa)	Hardness (HV)	Hardness (HV)
Ni	471	201	60	64	65
FeNi	609	249	192	116	64
FeNiCo	621	245	147	112	78
FeNiCoCr	933	403	189	132	85
FeNiCoCrMn	821	367	156	129	137
Nb[a]	376	180	207	80	135
TiNb	495	191	574	179	117
TiNbHf	1009	330	857	290	137
TiNbHfTa	1069	369	783	307	125
TiNbHfTaZr	1046	377	985	327	119

[a] As-received rod.

Fig. 5 (b) presents the relationship between dislocation density and mechanical properties (compressive yield strength and hardness for the *bcc* Ti-Nb-Hf-Ta-Zr family samples), and the values are listed in Table 2. The magnitudes of the yield strength and hardness varied with the level of dislocation density. The significant increases in the hardness and yield strength were observed from the binary TiNb and ternary TiNbHf alloys, which are resulted from the significant increase in dislocation density. The levels of dislocation density for the TiNbHf, TiNbHfTa and TiNbHfTaZr alloys were significantly different but their yield strength and hardness were similar. According to equation (4), the interaction between dislocations and shear modulus impacts the strength of

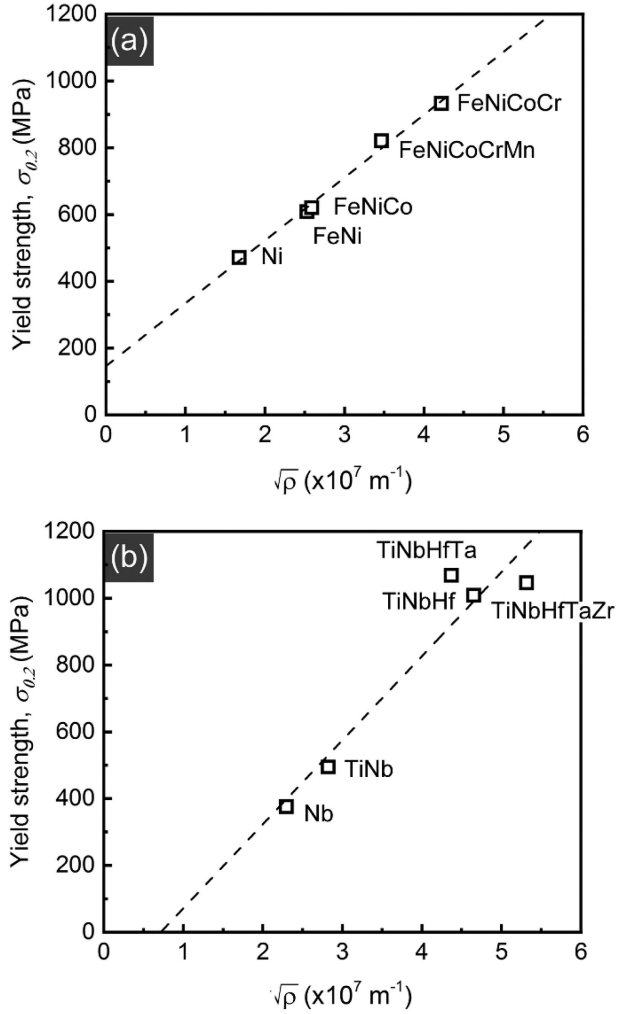

Fig. 6. Relationship between yield strength and square root of dislocation density ($\sqrt{\rho}$) for (a) the as-swaged *fcc* Fe-Ni-Co-Cr-Mn family samples and (b) the as-swaged *bcc* Ti-Nb-Hf-Ta-Zr family samples.

materials. Among the constituent elements of the Ti-Nb-Hf-Ta-Zr family samples, Ta has the largest value of shear modulus (69 GPa) whereas those of other constituent elements are between 30 and 40 GPa [20]. The higher values of yield strength and hardness is possibly led by higher shear modulus of the TiNbHfTa alloy than the TiNbHf alloy. The lower value of shear modulus in the TiNbHfTaZr HEA may results in similar levels of the yield strength and hardness between the TiNbHfTa and TiNbHfTaZ alloys.

Based on the Taylor relationship in equation (4), the relationship between compressive yield strength ($\sigma_{0.2}$) and the square root of the total dislocation density ($\sqrt{\rho}$) are plotted in Fig. 6 (a) and (b). Fig. 6 (a) shows the relationship for the *fcc* Fe-Ni-Co-Cr-Mn family samples. A linear fitting on the data points implies that the work hardening behavior of the FeNiCoCrMn HEA is equivalent to its sub-alloys and pure Ni sample. For the results in Fig. 6(a), taking the y-intercept from the linear fitting, the value of friction stress σ_0 (describing resistance to dislocation motion at dislocation-free state) is determined to be 146 MPa. The calculated friction stress value is in good agreement with experimental yield strength of the FeNiCoCrMn HEA after annealing in which the residual stresses is eliminated (~156 MPa) [23]. Moreover, the yield strength of the *fcc* samples at as-annealed state were between 147 and 192 MPa [23] as listed in Table 2. The friction stress at dislocation-free state can be equivalent to the level of solid solution hardening. In a comparison with hardness calculated by rule of mixtures (ROM) using the hardness of pure elements at room temperature [32], the experimental values of hardness at as-annealed state are not significantly different as shown in Table 2. This suggests that the levels of solid solution hardening for the *fcc* alloys are not significantly large [33]. A large increase in the yield strength of these alloys after cold deformation demonstrates a large work hardening effect. From equation (4), the slope of the fit line in Fig. 6 (a) is a value of $M\alpha Gb$ term. The average values of shear modulus G (~80.40 GPa) and Burgers vector b (~2.523 Å) were taken to extract the interaction coefficient α value. The α value for the *fcc* Fe-Ni-Co-Cr-Mn family samples was determined to be 0.3. This value lies in the range of 0.3–0.5, which is reported for conventional metals [34,35]. In many studies, the α value of 0.3 is used for modelling of work hardening in typical *fcc* metals [35]. The dislocation interaction coefficient α is generally defined by a number of parameters i.e. dislocation distribution, alloying, deformation mode, temperature and crystal orientation [36]. The good linear fitting result and the extracted α value suggest that the work hardening behavior of the FeNiCoCrMn HEA is consistent with its sub-alloys as well as typical *fcc* metals.

For the *bcc* Ti-Nb-Hf-Ta-Zr family samples, the relationship between compressive yield strength and the square root of the total dislocation density is plotted in Fig. 6 (b). The y-intercept (defined as lattice resistance, σ_0) from the linear fitting on the data points is negative (−179 MPa). This negative value is probably resulted from large differences in the lattice resistance of TiNbHfTaZr HEA and its sub-alloys. Our experimental yield strengths of as-annealed Nb, TiNb, TiNbHf, TiNbHfTa and TiNbHfTaZr are widely different and are 207, 574, 857, 783 and 985 MPa, respectively, as listed in Table 2 [23]. The levels of solid solution hardening are larger than the *fcc* Fe-Ni-Co-Cr-Mn family samples and largely different depending on the composition and the level of lattice distortion [23]. Furthermore, other works state that the solid solution hardening plays a dominant role in the mechanical properties of refractory high entropy alloys (e.g. TiNbHfTaZr, MoNbTaV, MoNbTaW) based on the fact that hardness measurements showed that 3–5 times larger values than the values estimated by ROM [37,38]. The hardness estimated by ROM for the studied *bcc* samples are calculated from the hardness of pure element at room temperature [39] as listed in Table 2 and much smaller than our experimental values of hardness at as-annealed state [23]. The model of solid solution hardening, which considers the elastic interactions between the local stress field of solute atoms and those of dislocations, is applied to an estimation of the hardness and yield strength in refractory high entropy alloys [37]. The estimated values for the TiNbHfTaZr HEA are 331 HV of hardness and 1080 MPa of yield strength [37]. These estimated values are similar to the experimental values of the cold-worked sample in this study as shown in Table 2, and these large values indicate a strong effect of solid solution hardening in the TiNbHfTaZr HEA. It can be said that the role of work hardening in the TiNbHfTaZr HEA and its sub alloys gives a less impact on the mechanical properties than the role of solid solution hardening. Besides the different levels of solid solution hardening among the *bcc* Ti-Nb-Hf-Ta-Zr family samples, a change in slope or non-linear behavior could lead to the negative value of the y-intercept due to more complex dislocation mechanism in the studied *bcc* samples. In literature, the αvalue for the TiNbHfTaZr HEA is approximately 0.16 [40] and the α value of polycrystalline niobium is 0.47 [40]. These works and the finding in this study indicate that dislocation-dislocation interactions for the TiNbHfTaZr HEA is different from Nb metals and possibly other sub-alloys. It can be assumed that the work hardening behaviors of the *bcc* Ti-Nb-Hf-Ta-Zr family samples are different.

4. Summary

The level of dislocation accumulation after cold rotary swaging with 85–90% area reduction has been studied in two different crystal structure types of single solid solution phase high entropy alloys (HEAs): *fcc*-structured FeNiCoCrMn and *bcc*-structured TiNbHfTaZr

HEAs.

The quantitative analysis of dislocation density shows that the values of dislocation density for all studied samples lie in a range between 10^{14} - 10^{15} m^{-2}, which is in agreement with probable range of dislocation density in severely deformed metallic materials. The level of dislocation density after cold deformation varies as a function of various parameters such as solid solution effect associated with the compositional complexity, atomic size misfit in determination of lattice distortion, staking fault energy and melting point. The higher degree in the compositional complexity and the more barriers to dislocation motions produced by lattice distortion lead to higher dislocation accumulation. The lower stacking fault energy and lower homologous temperature associated with higher melting point also increase dislocation accumulation. The level of dislocation density is proportional to atomic size misfit in a determination of lattice distortion, i.e., the atomic size misfit dominates the level of dislocation accumulation during the cold plastic deformation. In a comparison with the sub-alloys of each alloy system, the *fcc*-structured FeNiCoCrMn and *bcc*-structured TiNbHfTaZr HEAs reveal the high levels of dislocation density after cold swaging due to their compositional complexity, large atomic size misfit and other intrinsic properties.

The mechanical properties in terms of microhardness and compressive yield strength are proportional to the level of dislocation density. The analysis of work hardening behaviors based on Taylor relationship suggests that dislocation-dislocation interaction of the FeNiCoCrMn HEA are similar to its sub-alloys and pure Ni sample. For the *bcc* Ti-Nb-Hf-Ta-Zr family samples, the dislocation interaction varies depending on the alloy compositions.

Declaration of competing interest

The authors declare that they have no known competing financial interests or personal relationships that could have appeared to influence the work reported in this paper.

Acknowledgement

This research work was financially supported mainly by the Deutsche Forschungsgemeinschaft DFG (HA7796/1-1) and Graduate Academy of TU Dresden. Authors also acknowledge the support of the Basic Research Laboratory Program through the Ministry of Education of the Republic of Korea (2019R1A4A1026125) and the National Research Foundation of Korea (NRF) grant funded by the Korea government (MSIT) (NRF-2020R1F1A1076636 and NRF-2020R1C1C1005553). The authors thank Prof. Dr. J. Freudenberger, C. Blum, D. Seifert and S. Donath for experimental supports and technical assistances at the IFW-Dresden. Portions of this research were carried out at High Resolution Powder Diffraction Beamline P02.1 of the DESY in Hamburg, Germany.

Appendix A. Supplementary data

Supplementary data to this article can be found online at https://doi.org/10.1016/j.pnsc.2020.07.002.

References

[1] R. Kozak, A. Sologubenko, W. Steurer, Z. für Kristallogr. - Cryst. Mater. 230 (1) (2015) 55–68.
[2] E.J. Pickering, N.G. Jones, Int. Mater. Rev. 61 (3) (2016) 183–202.
[3] B. Cantor, I.T.H. Chang, P. Knight, A.J.B. Vincent, Mater. Sci. Eng. 375–377 (2004) 213–218.
[4] J.W. Yeh, S.K. Chen, S.J. Lin, J.Y. Gan, T.S. Chin, T.T. Shun, C.H. Tsau, S.Y. Chang, Adv. Eng. Mater. 6 (5) (2004) 299–303.
[5] M. Walbrühl, D. Linder, J. Ågren, A. Borgenstam, Mater. Sci. Eng. 700 (Supplement C) (2017) 301–311.
[6] M.C. Gao, J.W. Yeh, P.K. Liaw, Y. Zhang, High-entropy Alloys: Fundamentals and Applications, Springer Nature, Switzerland, 2016.
[7] H.Y. Diao, R. Feng, K.A. Dahmen, P.K. Liaw, Curr. Opin. Solid State Mater. Sci. 21 (5) (2017) 252–266.
[8] C. Varvenne, A. Luque, W.A. Curtin, Acta Mater. 118 (Supplement C) (2016) 164–176.
[9] A. Gali, E.P. George, Intermetallics 39 (2013) 74–78.
[10] Z.P. Lu, H. Wang, M.W. Chen, I. Baker, J.W. Yeh, C.T. Liu, T.G. Nieh, Intermetallics 66 (2015) 67–76.
[11] F. Otto, A. Dlouhý, C. Somsen, H. Bei, G. Eggeler, E.P. George, Acta Mater. 61 (15) (2013) 5743–5755.
[12] J.P. Couzinié, L. Lilensten, Y. Champion, G. Dirras, L. Perrière, I. Guillot, Mater. Sci. Eng. 645 (2015) 255–263.
[13] S. Gorsse, J.-P. Couzinié, D.B. Miracle, Physics 19 (8) (2018) 721–736 C.R.
[14] G. Laplanche, O. Horst, F. Otto, G. Eggeler, E.P. George, J. Alloys Compd. 647 (2015) 548–557.
[15] S.-J. Lim, K.-H. Na, H.-J. Choi, Y.-B. Park, C.-H. Lee, Proc. Inst. Mech. Eng. Part B J. Eng. Manuf. 221 (9) (2007) 1401–1406.
[16] J. Gubicza, X-ray Line Profile Analysis in Materials Science, IGI Global, 2014.
[17] A. Khorsand Zak, W.H. Abd Majid, M.E. Abrishami, R. Yousefi, Solid State Sci. 13 (1) (2011) 251–256.
[18] G.K. Williamson, R.E. Smallman, Phil. Mag. 1 (1) (1956) 34–46.
[19] P. Bordet, EPJ Web Conf. 104 (2015) 01003-1-14.
[20] M. Winter, 2018, 2018. http://www.webelements.com.
[21] P. Thirathipviwat, G. Song, J. Jayaraj, J. Bednarcik, H. Wendrock, T. Gemming, J. Freudenberger, K. Nielsch, J. Han, J. Alloys Compd. 790 (2019) 266–273.
[22] L.R. Owen, E.J. Pickering, H.Y. Playford, H.J. Stone, M.G. Tucker, N.G. Jones, Acta Mater. 122 (2017) 11–18.
[23] P. Thirathipviwat, Microstructure, Lattice Strain and Mechanical Properties of Single Phase Multi-Component Alloys, Doctoral Disseration, Dresden University of Technology, 2019.
[24] H. Parvin, M. Kazeminezhad, Comput. Mater. Sci. 95 (2014) 250–255.
[25] H. Song, F. Tian, Q.-M. Hu, L. Vitos, Y. Wang, J. Shen, N. Chen, Phys. Rev. Mater. 1 (2) (2017) 023404.
[26] I.L. Dillamore, E. Butler, D. Green, Metal Sci. J. 2 (1) (1968) 161–167.
[27] F.R.S.G.I. Taylor, Proc. Royal Soc. London. Series A 145 (855) (1934) 362.
[28] G. Yang, S.-J. Park, Materials 12 (12) (2019) 2003.
[29] C. Cáceres, P. Lukáč, Philos. Mag. A 88 (7) (2008) 977–989.
[30] W.F. Hosford, Mechanical Behavior of Materials, Cambridge University Press, Cambridge, 2005.
[31] J.M. Rosenberg, H.R. Piehler, Metall. Trans. 2 (1) (1971) 257–259.
[32] ASM International Handbook Committee, ASM Handbook Volume 2: Properties and Selection: Nonferrous Alloys and Special-Purpose Materials, ASM International, 1992.
[33] Y. Zhang, High-entropy Materials: a Brief Introduction, Springer, 2019.
[34] K.K. Chawla, M. Meyers, Mechanical Behavior of Materials, Prentice Hall Upper, Saddle River, 1999.
[35] E. Nes, Prog. Mater. Sci. 41 (3) (1997) 129–193.
[36] F.F. Lavrentev, Mater. Sci. Eng. 46 (2) (1980) 191–208.
[37] H.W. Yao, J.W. Qiao, J.A. Hawk, H.F. Zhou, M.W. Chen, M.C. Gao, J. Alloys Compd. 696 (2017) 1139–1150.
[38] H.W. Yao, J.W. Qiao, M.C. Gao, J.A. Hawk, S.G. Ma, H.F. Zhou, Y. Zhang, Mater. Sci. Eng. 674 (2016) 203–211.
[39] O.N. Senkov, J.M. Scott, S.V. Senkova, D.B. Miracle, C.F. Woodward, J. Alloys Compd. 509 (20) (2011) 6043–6048.
[40] G. Dirras, H. Couque, L. Lilensten, A. Heczel, D. Tingaud, J.P. Couzinié, L. Perrière, J. Gubicza, I. Guillot, Mater. Char. 111 (2016) 106–113.